CCFE
CULHAM CENTRE FOR FUSION ENERGY

UK Atomic Energy Authority

UKAEA-CCFE-CP(23)61

L. Horvath, M. Maslov, P.A. Schneider, C.F. Maggi,
L.Frassinetti, B. Lomanowski, R.B. Morales, D. Nina,
S. Saarelma, J. Simpson, G. Corrigan, D.I. Refy,
M.Brix, T. Pereira, M. Vecsei, JET Contributors

Pedestal particle balance studies in JET-ILW H-mode plasmas

Pedestal particle balance studies in JET-ILW H-mode plasmas

L. Horvath, M. Maslov, P.A. Schneider, C.F. Maggi, L.Frassinetti, B. Lomanowski, R.B. Morales, D. Nina, S. Saarelma, J. Simpson, G. Corrigan, D.I. Refy, M.Brix, T. Pereira, M. Vecsei, JET Contributors

This paper has been submitted to
48th EPS Conference on Plasma Physics, Maastricht (Netherlands), June 27 to July 1 2022

Pedestal particle balance studies in JET-ILW H-mode plasmas

L. Horvath[1], B. Lomanowski[2], J. Karhunen[3,1], M. Maslov[1], P. A. Schneider[4], J. Simpson[1,5], M. Brix[1], B. Chapman-Oplopoiou[1], G. Corrigan[1], L. Frassinetti[6], M. Groth[5], K. Lawson[1], C. F. Maggi[1], S. Menmuir[1], R. B. Morales[1], D. Moulton[1], O. Myatra[1], D. Nina[7], T. Pereira[1], D. I. Réfy[8], S. Saarelma[1], M. Vécsei[8] and JET Contributors*

EUROfusion Consortium, JET, Culham Science Centre, Abingdon, OX14 3DB, UK
[1]United Kingdom Atomic Energy Authority, Culham Centre for Fusion Energy, Culham Science Centre, Abingdon, Oxon, OX14 3DB, UK
[2]Oak Ridge National Laboratory, Oak Ridge, Tennessee, US
[3]VTT Technical Research Centre of Finland, P.O. Box 1000, 02044 VTT, Finland
[4]Max-Planck-Institut für Plasmaphysik, Boltzmannstrasse 2, D-85748, Garching, Germany
[5]Aalto University, 02150 Espoo, Finland
[6]Division of Fusion Plasma Physics, KTH Royal Institute of Technology, Stockholm, Sweden
[7]Instituto de Plasmas e Fusao Nuclear, Instituto Superior Tecnico, Universidade Lisboa, Portugal
[8]Center for Energy Research, Budapest 1121, Hungary
*See the author list of "Overview of JET results for optimising ITER operation" by J. Mailloux et al. 2022 Nucl. Fusion 62 042026

E-mail: laszlo.horvath@ukaea.uk

Abstract.

JET-ILW type I ELMy H-modes at 2.5MA/2.8T with constant NBI heating (23 MW) and gas fuelling rate were performed, utilising ELM pacing by vertical kicks and plasma shaping (triangularity, δ) as tools to disentangle the effects of ELMs, inter-ELM transport and edge stability on the pedestal particle balance. In agreement with previous studies, the pedestal confinement improves with increasing δ, mostly due to a significant increase in pedestal density while the ELM frequency (f_{ELM}) is decreased. Improved pedestal confinement with increasing δ was observed even when the pedestal MHD stability was degraded artificially by vertical kicks, implying that increased triangularity may favourably affect the inter-ELM pedestal recovery. The workflow developed to quantify the pedestal particle balance uses high time-resolution profile reflectometry to characterise the inter-ELM evolution of the plasma particle content ($\mathrm{d}N/\mathrm{d}t$), the NEO drift-kinetic solver to evaluate the neoclassical fluxes and interpretative EDGE2D-EIRENE simulations to estimate the edge particle source. The edge particle source is then constrained by deuterium Balmer-α line intensity measurements in the main chamber, which are however strongly affected by reflections from the metal walls. The reflections are accounted for by the CHERAB code taking the divertor emission (the brightest light source in the torus) distribution from imaging

spectroscopy measurements as input. Our analysis shows that in the second half of the ELM cycle, the volume-integrated particle source is larger than $\mathrm{d}N/\mathrm{d}t$, indicating that transport plays a key role in the inter-ELM pedestal recovery.

1. Introduction

In an H-mode plasma [1] the confinement is improved due to the formation of a narrow transport barrier at the edge. Inside the transport barrier, the energy and particle transport are reduced, and a steep pressure gradient is formed, which gives rise to a pressure pedestal. The heightened edge pressure also leads to improved global confinement due to core profile stiffness [2, 3, 4, 5]. However, the steep pressure gradient can trigger edge localised modes (ELMs) [6], followed by a transient loss of energy and particles which are deposited onto the plasma facing components. Understanding pedestal physics is essential to predict and optimise plasma performance in current and future tokamak experiments.

The H-mode pedestal is governed by at least three interacting processes: pedestal stability, transport and sources. The stability of the pedestal in a type I ELMy regime [6] is generally described by MHD theory [7]. The high pressure gradient and the edge current density at the edge drive Peeling-Ballooning (P-B) modes unstable [8, 9], triggering an ELM. P-B stability provides an ultimate limit on the pedestal pressure at the onset of the ELM, but the inter-ELM turbulent [10, 11, 12] and neoclassical [13, 14] transport, along with the sources, will determine the relative contributions from the pedestal density and temperature. The exact role of the edge particle source and pedestal transport in setting the density pedestal is still an open question [15]. Reduced pedestal models [16, 17, 18, 19, 20] have proven successful in predicting the pedestal electron pressure for a wide range of plasma scenarios, but they lack a first principle based, predictive model for the edge density.

In this study, we investigate the balance of particle sources and transport in the latter part of the ELM cycle where the pedestal recovery is typically slow compared to the transient crash and fast recovery phase [21, 22]. The evolution of the pedestal particle content is evaluated from detailed analysis of high resolution profile reflectometry data. The edge particle source is estimated by means of interpretative edge-scrape-of-layer (edge-SOL) fluid transport simulations using the EDGE2D-EIRENE code [23, 24, 25]. Comparison of these results allows an assessment of the contributions of sources and transport to edge particle balance. The role of MHD stability in the pedestal formation is also investigated.

The paper is organised as follows. Section 2 describes the analysed JET-ILW H-mode experiments and presents the comparison of pedestal density and temperature profiles. The analysis of the linear ideal MHD stability of the investigated pedestals is discussed in 3. The interpretative EDGE2D-EIRENE simulations to estimate the edge particle source is presented in section 4. The results on the balance of the source and

transport during the inter-ELM pedestal evolution is discussed in section 5, followed by the conclusions in section 6.

2. Experiments

In this work, we investigate JET-ILW type I ELMy H-mode experiments that utilised plasma shaping (triangularity) and ELM pacing by vertical kicks as tools to disentangle the effects of edge stability, ELMs and inter-ELM particle transport on the pedestal particle balance. It has been observed in several tokamak experiments, that the pedestal confinement typically improves with increasing triangularity [22, 26, 27, 28, 29, 30, 31, 32, 33, 34, 35]. In JET and ASDEX-Upgrade, the increase of pedestal pressure with triangularity, at otherwise fixed engineering parameters, is due to higher pedestal density being obtained for similar pedestal temperature [22, 26, 27, 28, 29, 31, 32]. It has also been reported from these two devices that the ELM frequency is reduced at higher triangularities [22, 26, 30, 31]. The beneficial effect of triangularity on the pedestal performance is typically associated with the improved stability of Peeling-Ballooning modes before the ELM event (pre-ELM) [8, 36, 37, 38]. Increased triangularity decouples peeling and ballooning modes opening up second stability access leading to a higher stability boundary.

The application of a fast and controlled vertical plasma motion (known as vertical kicks in JET) for frequency control of ELMs has been successfully demonstrated on several tokamaks [39, 40, 41, 42]. This method on JET relies on the vertical stabilization control system to drive the fast vertical plasma motion. Vertical kicks can trigger ELMs by introducing an intermittent, local perturbation of the current density close to the separatrix. If the current perturbation is large enough to destabilise the peeling component of the edge instability responsible for the ELM onset, an ELM is triggered before the pedestal would naturally reach the Peeling-Ballooning stability limit [39].

Comparative type I ELMy H-modes were performed at 2.5 MA plasma current and 2.8 T toroidal magnetic field with constant NBI (Neutral Beam Injection) power of 23 MW, no ICRH (Ion Cyclotron Resonance Heating) in the main heating phase‡ and constant deuterium gas fuelling rate at 4.4×10^{22} electron/s. A lower triangularity ($\delta = \delta_{\text{lower}} + \delta_{\text{upper}} = 0.2$) and a higher triangularity ($\delta = 0.3$) pulse with natural ELM frequency and a higher triangularity ($\delta = 0.3$) pulse with 36 Hz vertical kicks for ELM pacing were selected for detailed comparative analysis. The main waveforms of these three pulses are shown in figure 1. Strike point sweeping with 4 Hz frequency was introduced in these pulses for operational reasons, to reduce the heat load on the tungsten coated divertor tiles. This introduces oscillations in some of the measured plasma parameters.

‡ RF was not used in the main heating phase (which is the plasma analysed), but was used in the tail of the discharge for safe landing, to prevent disruption caused by core tungsten accumulation and thus radiative collapse during the plasma current ramp-down.

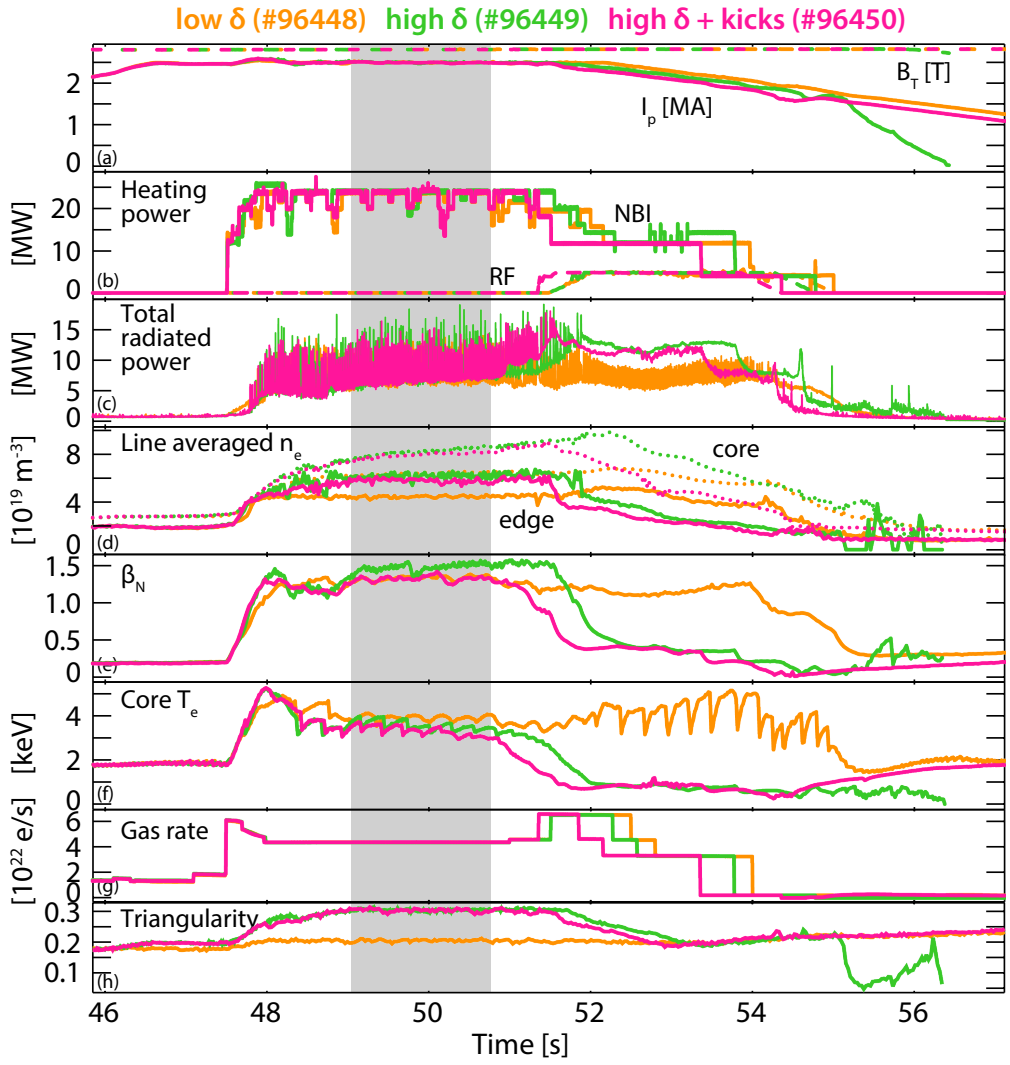

Figure 1. The main plasma parameters of the three representative discharges examined in this paper. The $\delta = 0.2$ plasma is shown in orange, the $\delta = 0.3$ in green and the $\delta = 0.3$ with kicks in magenta. The grey area indicates the analysed time interval. (a) The total plasma current, I_p and the toroidal magnetic field, B_t. (b) The NBI and ICRH heating power. (c) The total radiated power. (d) The core and edge line averaged density. (e) The normalised plasma β, β_N. (f) The core electron temperature. (g) The external D_2 fuelling gas rate. (h) The average plasma triangularity, $\delta = \delta_{\text{lower}} + \delta_{\text{upper}}$.

The ELM-averaged§ pedestal electron density (n_e) and temperature (T_e) profiles from Thomson scattering (TS) [43] and the ion temperature (T_i) profiles from the edge charge exchange spectroscopy (CXRS) system [44, 45] measuring Ne and C impurities are shown in figure 2. Besides the raw data points, figure 2 shows the modified tanh (mtanh) [46] fitted profiles as well. Figure 2c also shows the raw ion temperature data on the top of the mtanh fit of the electron temperature profiles (same as in figure 2) for

§ ELM-averaged means that profiles are averaged over ELMs. All of the profiles are taken from the steady phase of the discharge.

comparison of T_e and T_i. The ion and electron temperatures are similar at the pedestal top within the measurement uncertainties of the edge CXRS system, but T_i in the edge transport barrier and at the separatrix cannot be resolved.

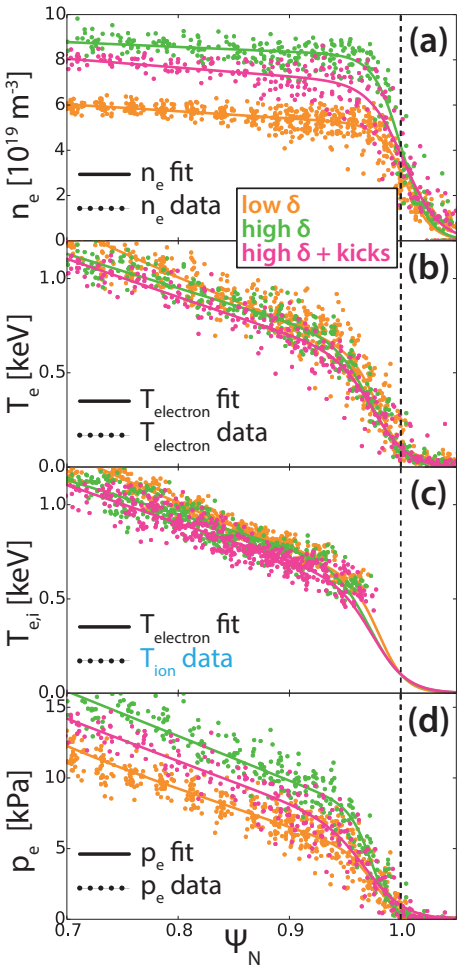

Figure 2. The ELM-averaged pedestal kinetic profiles for the three representative discharges examined in this paper. The $\delta = 0.2$ plasma is shown in orange, the $\delta = 0.3$ in green and the $\delta = 0.3$ with kick in magenta. (a) Electron density data from TS and corresponding mtanh fits. (b) Electron temperature data from TS and corresponding mtanh fits. (c) Ion temperature data from CXRS. The underlying solid lines are the mtanh fits of the TS electron temperature, same as in figure b. This is to confirm that $T_e \approx T_i$ at the pedestal top. (d) Electron pressure data from TS and corresponding mtanh fits. (The kinetic profiles are radially aligned so that the separatrix temperature is 100 eV.)

As shown in figure 2, the pedestal pressure significantly improves with increasing triangularity mostly due to an increase in pedestal density and the change in electron and ion temperatures is small. Also, the natural ELM frequency decreases from 39 Hz at $\delta = 0.2$ to 25 Hz at $\delta = 0.3$. When f_{ELM} is increased by vertical kicks at $\delta = 0.3$ to 37 Hz (close to the natural f_{ELM} of the $\delta = 0.2$ pulse), the pedestal density and thus the

pressure is somewhat decreased, but both still significantly higher than in the $\delta = 0.2$ case. This observation is discussed in view of the pedestal stability in the next section.

3. Pedestal MHD stability

The beneficial effect of increasing triangularity on pedestal performance is typically associated with the increased stability of Peeling-Ballooning modes that trigger type I ELMs [8, 36, 37, 38]. However, with the introduction of vertical kicks, the ELMs are triggered before the pedestal would naturally reach the MHD stability limit. In the $\delta = 0.3$ plasma with vertical kicks, the pedestal pressure is degraded (by ≈25 %) with respect to the $\delta = 0.3$ discharge with natural f_{ELM}. Despite this artificial degradation of the pedestal MHD stability, the pedestal pressure is still significantly higher (by ≈30 %) in the $\delta = 0.3$ kicked pulse compared to that of the $\delta = 0.2$ counterpart. This implies that increased plasma triangularity may also affect inter-ELM transport, and thus lead to increased pedestal confinement.

Ideal MHD stability of the pedestal was investigated with the HELENA fixed boundary equilibrium [47] and the ELITE ideal MHD stability codes [8, 9]. The $j - \alpha$ pedestal stability diagram for the three representative discharges is shown in figure 3, where α is the normalised pressure gradient‖ and j is the normalised current density. The HELENA equilibrium is self-consistent with respect to the current profile that was evaluated using Redl's bootstrap current formula [49] and assuming a fully diffused Ohmic current with neoclassical resistivity. The pre-ELM mtanh fitted TS data was used as input kinetic profiles, assuming $T_e = T_i$ (consistent with charge exchange measurements at the pedestal top) and line averaged Z_{eff} with Be as a single impurity. The kinetic profiles are radially aligned so that the separatrix temperature is 100 eV.

The Peeling-Ballooning (P-B) stability boundary (solid lines in figure 3) was evaluated using $\gamma_{\mathrm{MHD}} > 0.5 \times \omega_{\mathrm{dia}}$ as stability criterion, where γ_{MHD} is the linear growth rate and ω_{dia} is the diamagnetic frequency. The stability boundary is very similar for all three discharges. The increase in triangularity from 0.2 to 0.3 is too small to see a clear stabilisation effect on the stability boundary with increases triangularity. A small stabilising effect at $\delta = 0.3$ was observed when parameter differences between discharges (such as β_N, β_{pol}, volume, etc.) were removed and only the shaping effect was investigated.

The stars in figure 3 show the operational point of the pedestal as obtained in the experiment with their associated error bars derived from the uncertainty of the mtanh fit parameters. The operational points for the pulses with natural ELM frequency are close to the P-B boundary thus the ELM trigger is consistent with the P-B paradigm. The operational point is further from the stability boundary for the $\delta = 0.3$ pulse

‖ The normalised pressure gradient is defined as in [48]: $\alpha = \frac{-2\partial V/\partial\Psi}{(2\pi)^2}\left(\frac{V}{2\pi^2 R_0}\right)^{1/2}\mu_0\frac{\partial p}{\partial\Psi}$, where V is the volume enclosed by the flux surface, R_0 is the geometric centre of the plasma and Ψ is the poloidal flux.

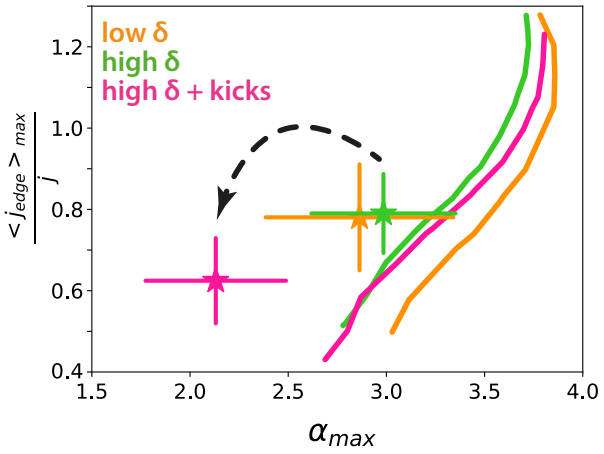

Figure 3. Liner MHD pedestal stability diagram for the three discharges analysed. The $\delta = 0.2$ plasma is shown in orange, the $\delta = 0.3$ in green and the $\delta = 0.3$ with kick in magenta. The operational points corresponding to the pre-ELM phase of the discharges are indicated with the stars and the respective error bars as a function of the normalised pressure gradient ($\alpha_{\max}$) and the normalised current density ($\langle j_{\rm edge}\rangle_{\max}/j$). The solid lines show the P-B stability boundary.

where vertical kicks were applied to increase $f_{\rm ELM}$. This is expected as the vertical kick introduces a current perturbation at the edge which triggers the ELM in conditions when the pedestal would otherwise still be stable to P-B modes. The P-B stability analysis used the equilibrium and kinetic profiles from this stable period preceding the triggered ELMs.

It was found that the pressure pedestal is wider in both $\delta = 0.3$ pulses than in the $\delta = 0.2$ case. This is shown in figure 4, where the edge pressure gradients are compared for the three pedestals. The wider pedestal at $\delta = 0.3$ allows for improved P-B stability and thus leads to higher pedestal pressure. This suggests that the improved pedestal pressure at higher δ is not necessarily a sole pre-ELM Peeling-Ballooning stability effect, but a change in inter-ELM transport could possibly play an important role in setting the higher density and thus higher pressure when the triangularity is increased.

4. Estimate of the edge particle source

The role of particle transport in the inter-ELM phase is studied in section 5 in more detail where the pedestal particle balance is discussed. In this section, we present the interpretative EDGE2D-EIRENE [23, 24, 25] simulations which were performed to estimate the edge particle source to examine the balance of source and transport in the pedestal. EDGE2D is a 2D fluid code with realistic geometry of the SOL and divertor region, which is coupled to EIRENE, a Monte Carlo code used to calculate the neutral particle distribution.

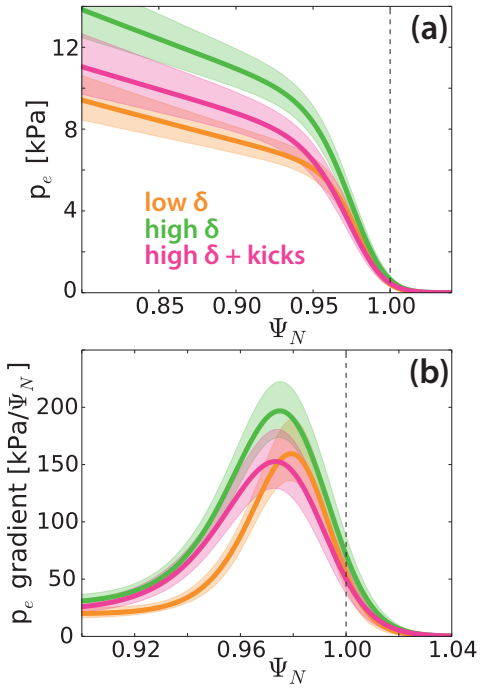

Figure 4. The mtanh fit of the pre-ELM electron pressure profile (a) and its gradient (b) for the three discharges analysed. The $\delta = 0.2$ plasma is shown in orange, the $\delta = 0.3$ in green and the $\delta = 0.3$ with kick in magenta. The error bars are derived from the uncertainty of the mtanh fit parameters. Note that while the pressure gradient is similar for the $\delta = 0.2$ and the $\delta = 0.3$ with kicks cases, α as shown in figure 3 is different. This is because the normalisation of the pressure gradient (α) also includes the plasma volume that is smaller for the $\delta = 0.3$ plasmas.

4.1. Simulation set-up and interpretative transport coefficients

We ran EDGE2D-EIRENE in interpretative mode, where the perpendicular transport coefficient of electron particle diffusion $D_\perp$ ($\Gamma_{e,\perp} = D_\perp \nabla_\perp n_e$), electron and ion heat transport $\chi_{e,i,\perp}$ ($q_{e,i,\perp} = -n_{e,i}\chi_{e,i,\perp}\nabla_\perp T_{e,i}$) and the divertor pump albedo were iterated until the solution fitted the measured inter-ELM ($40-80$ % fraction of the ELM cycle) upstream n_e and T_e profiles (measured by TS and the fast Li-beam emission spectroscopy (Li-BES) system [50]). The ion and electron heat transport coefficient profiles ($\chi_{e,\perp}$ and $\chi_{i,\perp}$) were assumed to be the same, due to lack of constraints to distinguish between them.

The separate contribution of ELM and inter-ELM transport was not studied with EDGE2D-EIRENE. The simulations were run until convergence, thus time independent solutions were obtained. The building up of the plasma stored energy between ELMs ($\mathrm{d}W/\mathrm{d}t$), that is equivalent to the ELM power loss (P_{ELM}), was not taken into account in the time-independent simulations. Thus, the input power in EDGE2D-EIRENE was set to the power crossing the separatrix inter-ELM ($P_{\mathrm{inter-ELM}} = P_{\mathrm{sep}} - P_{\mathrm{ELM}}$).

Cross-field drifts and a particle pinch term were not introduced in these simulations. The edge particle pinch may have an important role in the particle transport [51, 52, 53],

but in time independent simulations the experimental n_e profile could be reproduced with different variations of the diffusion coefficient and the pinch velocity, due to the lack of constraints. Thus, the particle diffusion coefficient here is regarded as an effective parameter describing the transport needed to exhaust the particle source from the plasma.

The grid for EDGE2D is generated such that it is aligned to the plasma equilibrium reconstructed using kinetic EFIT [54]. The grid extends to $\sim 10 - 15$ cm inside the separatrix towards the core plasma. The gas fuelling rate and location was set in accordance with the experiment. The experimental NBI fuelling rate was estimated using the PENCIL code [55], although this was found to be small compared to the neutral flux crossing the separatrix. The divertor configuration around the outer strike point cannot be modelled precisely in EDGE2D-EIRENE. The wall structure had to be slightly modified around the outer strike-point so that the grid does not cross wall surfaces, as described in [56] in more detail.

4.2. EDGE2D-EIRENE solutions

As described above, the perpendicular transport coefficients were iterated until the experimental upstream kinetic profiles could be matched. However, it has been found that multiple sets of transport coefficients can reproduce the kinetic profiles within the experimental uncertainty without simultaneously constraining the main chamber recycling. This is shown in figure 5, where the transport coefficients and the corresponding upstream n_e and T_e profiles are shown for the $\delta = 0.2$ discharge. For these four simulations, all the input parameters were kept the same except for the perpendicular transport coefficients. It is shown in figure 5, that the particle diffusion coefficient is changing by an order of magnitude in the pedestal and the SOL, while the heat transport coefficient is changing by a factor of 3 in the pedestal. Regardless of this significant variation in the perpendicular transport, the upstream profiles stay virtually the same. It is important to note that the divertor target quantities did not vary significantly either in this scan. The variation in j_{sat}, n_e and T_e at the outer target was between ± 30 %. For the inner target, the high $D_\perp$ case is significantly colder, but the other 3 cases are also within ± 30 % variation in terms of j_{sat}, n_e and T_e.

The above behaviour can be understood by examining the role of main chamber recycling in fuelling the plasma. The recycling flux is determined by ion flux arriving to the edge of the EDGE2D plasma grid. The recycling coefficient was set to 1 in these simulations (except for the pumping surfaces in the divertor), thus all particles are recycled as neutrals. By increasing the particle diffusion coefficient, the ion flux arriving at the edge of the plasma and at the wall surfaces is also increased, resulting in a higher recycling flux. The increased recycling flux leads to a higher neutral density and such increased particle source and it is this increased particle source in the plasma that compensates the effect of increased particle transport. In this way, multiple sets of particle diffusion coefficients can reproduce very similar upstream kinetic profiles.

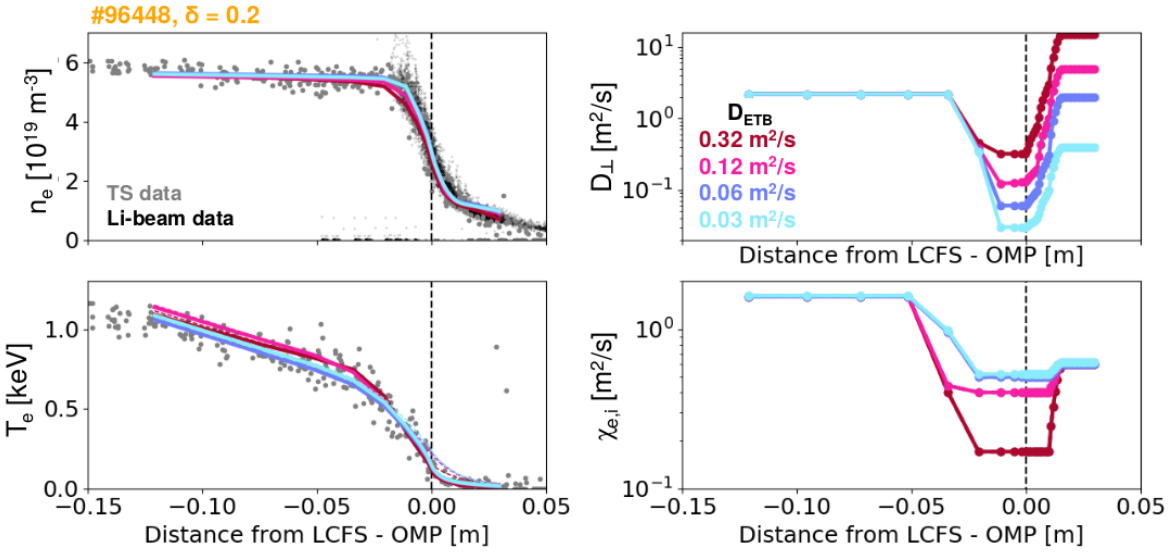

Figure 5. Inter-ELM TS profiles for n_e and T_e (in grey) and Li-BES data for n_e in the SOL (in black) in the steady phase of the $\delta = 0.2$ discharge. The upstream n_e and T_e profiles of the interpretative EDGE2D-EIRENE simulations with different set of $D_\perp$ coefficients are shown in colour. The simulations are labelled with the corresponding $D_\perp$ value inside the edge transport barrier, $D_{\perp,\mathrm{ETB}}$.

It is therefore necessary to also constrain the main chamber particle source, so as to extract the unique set of $D_\perp$ and $Chi_\perp$ profiles that matches the investigated pedestal. Figure 6 shows the ionisation source inside the separatrix as a function of $D_{\perp,\mathrm{ETB}}$ for the four simulations presented in figure 5. It can be seen that for these cases, the pedestal source is close to linearly increasing with $D_{\perp,\mathrm{ETB}}$ resulting in similar upstream density and temperature profiles (as shown in figure 5) despite the different set of transport coefficients. This also means that additional simulation constraints that carry information on the neutral density in the main chamber are needed to estimate the pedestal particle source.

4.3. Main chamber D_α line radiation constraint in EDGE2D-EIRENE

In order to constrain the pedestal particle source, we compared the emitted deuterium Balmer-α (D_α) radiation by the main chamber plasma in the EDGE2D-EIRENE simulation to that of the experimental measurements. The line-of-sight (LOS) of the corresponding spectrometer is crossing the plasma in the main chamber, but not in the divertor as shown in figure 7c. In this way, the measured line intensity carries direct information about the ionisation source in the SOL and the pedestal, but it does not integrate through the orders of magnitude brighter divertor emission. However, the D_α emission from the divertor is reflected by the JET-ILW metallic walls [57], hence it is captured along the horizontal LOS making significant contribution to the measured line intensity. Thus reflections need to be taken into account in the analysis by forward modelling.

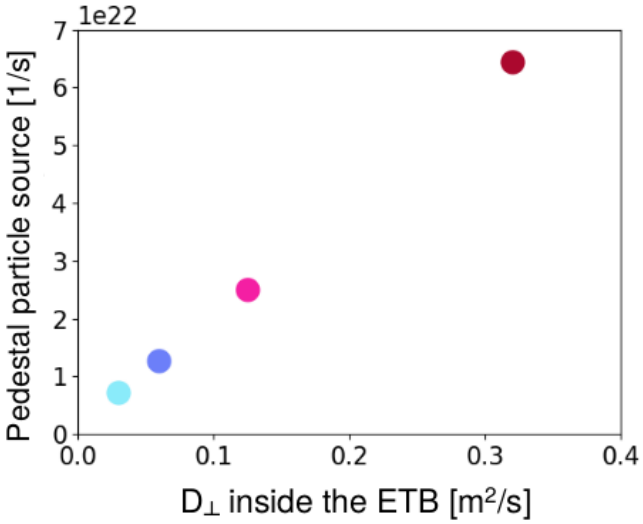

Figure 6. The particle source integrated over the plasma volume inside the separatrix is shown as a function of $D_{\perp,\mathrm{ETB}}$ inside the edge transport barrier (ETB) for the four interpretative EDGE2D-EIRENE simulations with different set of $D_\perp$ coefficients (#96448, $\delta = 0.2$).

To estimate the effect of reflections on the measured signal, the experimental D_α brightness in the divertor was taken from imaging spectroscopy measurements [58]. Imaging spectroscopy provided a time-averaged (during the inter-ELM phases over the steady phase of the discharge), 2D tomographic reconstruction of the D_α line intensity distribution in the divertor. The contribution of the reflected light from the divertor to the horizontal D_α line intensity measurement was estimated using the CHERAB code [59, 60] as illustrated in figure 7c. CHERAB includes definitions of the full JET-ILW machine geometry and estimates of the metallic tile spectral bidirectional reflectance distribution functions. It uses the RAYSECT [61] raytracing engine to provide estimates for the reflected light intensity. We used the experimental divertor D_α emission as input for CHERAB, assuming zero emission from the main chamber. In this we way, the background reflected emission of the measured D_α intensity on the horizontal LOS can be approximated.

The measured D_α light intensity as function of time is shown in grey in figure 7. The difference of the measured signal and the background reflected emission provides an estimate for the line intensity emitted by the plasma in the main chamber (the SOL and the pedestal). These estimated main chamber D_α line intensities are shown in figure 7a and 7b in black for the steady phase of the $\delta = 0.2$ and $\delta = 0.3$ natural f_{ELM} discharges after removing the spikes caused by ELMs. The obtained signal suffers from large oscillations, in part due to the applied strike point sweeping, which increases the uncertainty on this method to constrain the neutral density in the plasma. Nonetheless, this experimental comparison provides a sanity check on the overall level of main

chamber D_α emission in EDGE2D-EIRENE simulations and thus excludes some of the solutions obtained with unrealistic level of particle source in the pedestal and SOL.

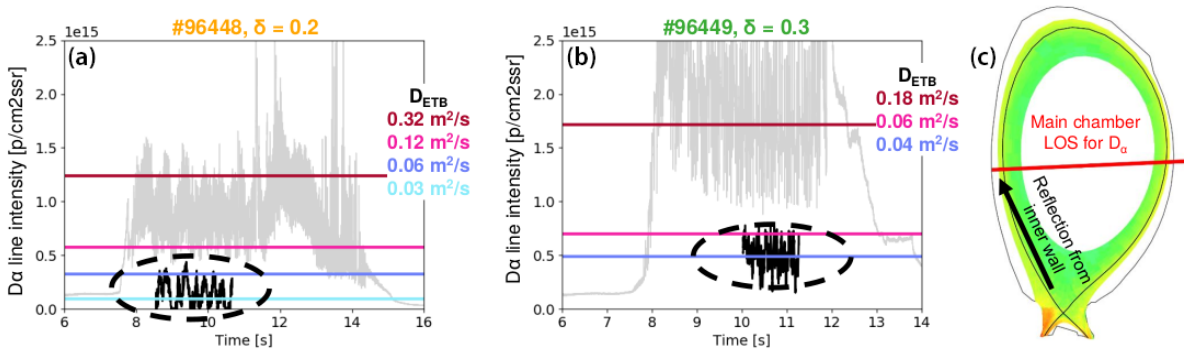

Figure 7. The measured D_α light intensity as function of time is shown in grey for the $\delta = 0.2$ and $\delta = 0.3$ natural f_{ELM} discharges. The signals after the removal of ELMs and offsetting the reflected light are shown is black. The synthetic D_α line intensities for the corresponding main chamber LOS are shown in colour from the EDGE2D-EIRENE solutions using different set of transport coefficients.

To compare with the estimated experimental main chamber D_α line intensities, synthetic diagnostic data was produced from the EDGE2D-EIRENE solutions by evaluating (using ADAS atomic data [62]) and integrating the D_α emission along the diagnostic LOS. This is shown in figure 7a and b with the coloured lines. It is seen that for the simulations using higher $D_\perp$ values, the synthetic D_α emission is too high compared to the experimental estimates. Thus, the simulations flagged as $D_{\perp,\mathrm{ETB}} = 0.03$ m^2/s and 0.06 m^2/s for the $\delta = 0.2$ case, and $D_{\perp,\mathrm{ETB}} = 0.04$ m^2/s and 0.06 m^2/s for the $\delta = 0.3$ case are the ones deemed experimentally feasible solutions.

Since the measured D_α emission along the horizontal LOS is dominated by reflections form the divertor, unfortunately it is not possible to select a unique solution from the EDGE2D/EIRENE simulations and thus fully constrain the evaluation of the edge particle source. Nevertheless, in the next section, we discuss the balance of the source and transport during the inter-ELM pedestal evolution in view of the above, experimentally feasible EDGE2D-EIRENE solutions with the consideration of the large uncertainty on the pedestal particle source.

5. The balance of the source and transport during the inter-ELM pedestal evolution

The main aim of these investigations is to characterise the balance of sources and transport that sets the density pedestal. In current tokamak experiments, the dominant particle fuelling in the pedestal comes from the ionisation of neutral atoms penetrating into the confined region. The particle transport occurs via different channels, such as ELM losses, neo-classical and turbulent transport. Our aim is to estimate the

contribution of these different channels. For this, the transient nature of ELMs needs to be considered as well.

Figure 8a shows the time evolution of the particle content (offset to 0 at the ELM onset) evaluated from profile reflectometry during an ELM cycle for the low $\delta = 0.2$ and $\delta = 0.3$ natural f_{ELM} pulses. At the ELM crash, significant amount of particles is lost from the plasma. But most of the lost particles are quickly recovered. The end of this "fast" recovery phase is indicated with the black vertical dashed line in figure 8a. The fast recovery is supposedly driven by an increased recycling flux as a result of the increased particle flux arriving to the divertor targets and limiter as a result of the ELM crash [63]. A sign of this increase in particle source can be seen in the spectroscopy data. The signals in figure 8b show the D_α light intensity in the main chamber. As discussed in section 4, the quantitative interpretation of this signal is challenging, but it shows that qualitatively the ionisation source in the main chamber is increased following the ELM crash.

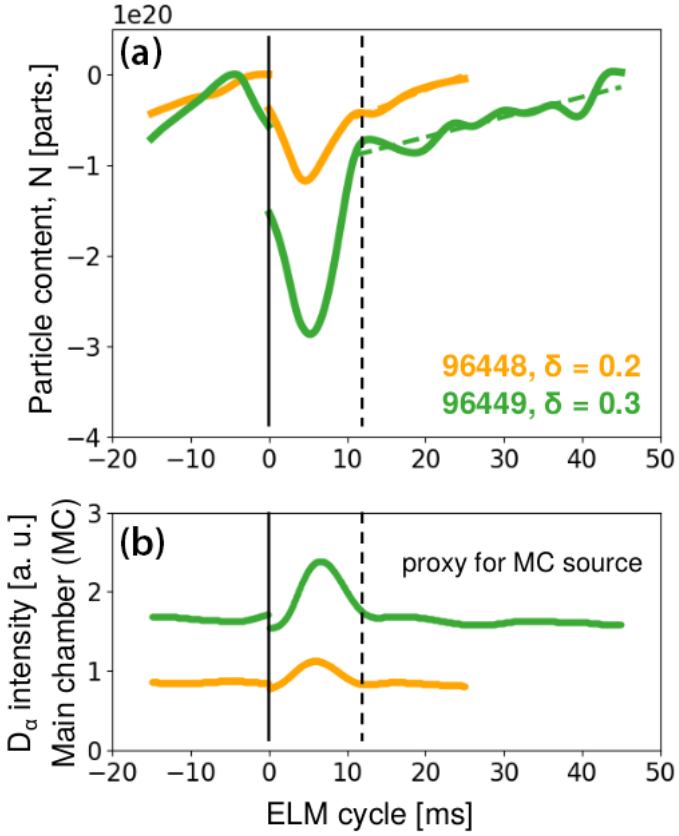

Figure 8. (a) Time evolution of the particle content during an ELM cycle (offset to 0 at the ELM onset) and (b) time evolution of the D_α light intensity in the main chamber during an ELM cycle for the low $\delta = 0.2$ and $\delta = 0.3$ natural f_{ELM} pulses.

The "fast" recovery phase is followed by a slower and longer phase (to the right of the horizontal dashed line). In the slower recovery phase, the main chamber D_α light intensity is more or less constant. We focus on the slow recovery phase to study the

pedestal particle balance. Thus, we are examining the pedestal particle balance in this phase assuming that the rate of change of the particle content ($\mathrm{d}N/\mathrm{d}t$) is a result of the difference between the constant source (S) and transport (T) terms:

$$\mathrm{d}N/\mathrm{d}t = S - T \ . \tag{1}$$

The question we seek to answer is to see whether the pedestal recovery is dominated by the source or the transport. $\mathrm{d}N/\mathrm{d}t$ is evaluated from the experimentally measured evolution of the particle content using high resolution profile reflectometry. The source is taken from the experimentally relevant EDGE2D-EIRENE simulations from section 4. Transport is calculated as a difference between the source and $\mathrm{d}N/\mathrm{d}t$. The transport channel is then further divided into contributions from neo-classical and turbulent transport by estimating the neo-classical particle flux using the NEO drift-kinetic code [64, 65]. Note that the turbulent particle flux is not modelled in this work, it is simply deducted from eq. (1), assuming that the total transport (T) is the sum of the neo-classical and turbulent fluxes.

The bar charts in figure 9 compare the magnitude of the source with that of the transport for the two investigated plasmas ($\delta = 0.2$ in figure 9a and $\delta = 0.3$ in figure 9b). We show two results for both plasmas. These represent the estimated particle source from the "experimentally relevant" EDGE2D-EIRENE simulations as shown in figure 7. We regard the two solutions (for each pulse) as a lower and upper bound estimate for the particle source, and the corresponding transport flux is calculated respectively using the experimentally measured $\mathrm{d}N/\mathrm{d}t$.

For the $\delta = 0.3$ pulse (figure 9b), it is clear that both the source and transport terms are relevant and the difference of these two large terms results in a small $\mathrm{d}N/\mathrm{d}t$. The particle flux is further divided into the contribution from neo-classical and turbulent transport. This suggests that the role of turublent transport is important in the evolution of the pre-ELM pedestal and it cannot be neglected. In the case of the $\delta = 0.2$ discharge, the picture is less clear. Due to the uncertainties on the main chamber D_α radiation constraint, the lower and upper bound solutions are very different. In the $D_{\perp,\mathrm{ETB}} = 0.03$ m^2/s case the source seems to be dominant over transport, but in the $D_{\perp,\mathrm{ETB}} = 0.06$ m^2/s case the source and transport terms are comparable. In summary, we conclude that the role of turbulent particle transport, in the pulses analysed, cannot be neglected from the pedestal particle balance. But, further improvements required both in spectroscopic measurements and edge transport simulations to be able to quantitatively compare the pedestal particle balance between different pedestals.

6. Discussion and conclusions

In the present paper, the pedestal particle balance and the role of pedestal MHD stability have been investigated in JET-ILW type I ELMy H-mode plasmas at different triangularities and ELM frequency. The enhanced pedestal confinement at high triangularity is typically associated with improved Peeling-Ballooning stability in the

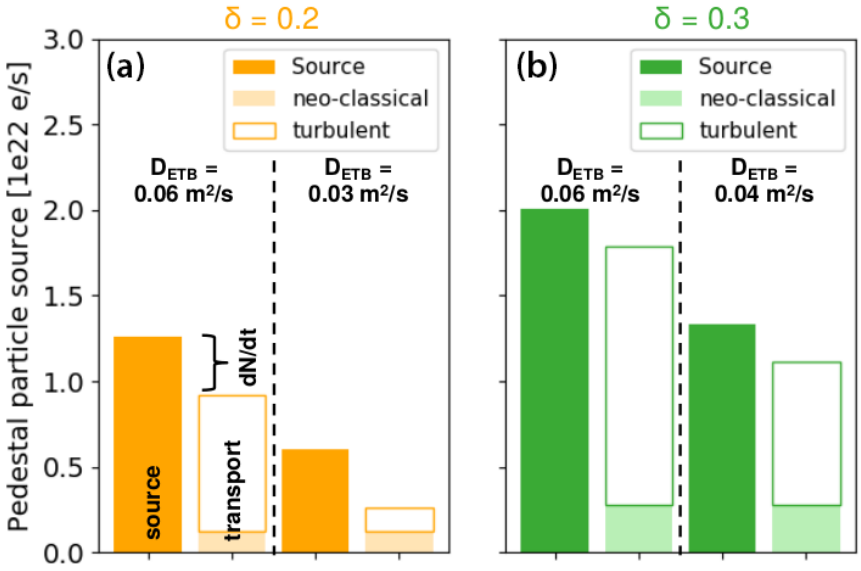

Figure 9. Comparison of the source and transport in the pedestal for the "experimentally relevant" EDGE2D-EIRENE solutions for the two investigated plasmas. (a) $\delta = 0.2$ in orange, (b) $\delta = 0.3$ in green.

pre-ELM phase [8, 36, 37, 38]. In contrast to this, we have observed that the pedestal pressure is higher at higher δ even when the pedestal stability is artificially degraded by introducing vertical kicks. This is likely due to the increased width of the pedestal at higher δ that allows for higher pedestal pressure at similar pressure gradient. The physical mechanism responsible for the wider pedestal has not been investigated in this work, but a change in inter-ELM pedestal transport as a result of enhanced shaping could be one candidate to explain these observations. Unfortunately the workflow presented in this work cannot provide quantitative comparative evidence of transport between the pedestals with different triangularities as the estimate on the pedestal particle source is too uncertain.

The literature contains several gyrokinetic studies about how plasma shaping affects core turbulence [66, 67, 68], but we have not found any systematic study investigating the effect of triangularity on pedestal turbulent transport. In Ref. [66], Belli mentions that nonlinear gyrokinetic simulations of core turbulence capture some of the shaping effects found experimentally, but they do not completely explain the degree of this dependence on triangularity. It may be that much of the experimentally observed strong triangularity dependence comes from the edge turbulence, which sets the boundary conditions for core transport.

Due to the lack of direct measurement of the neutral density, unravelling the role of the edge particle source and transport in setting the density pedestal structure is highly challenging. In current tokamaks, the characterisation of the neutral source is essential to understand the formation of the density pedestal structure, as also suggested

by several studies [15, 69, 70, 71]. In this work, we used edge-SOL transport simulations (EDGE2D-EIRENE), together with various plasma measurements for the estimation of the edge particle source. Comparing the estimated pedestal particle source with the experimentally inferred evolution of the pedestal particle content inter-ELM, we found that the role of turbulent particle transport, in general, cannot be neglected from the pedestal particle balance. Cases exist where a large source term is balanced by a large transport term resulting in a relatively slow recovery of the pedestal. This implies that for detailed pedestal prediction, the properties of both the particle source and transport need to be characterised.

In the EDGE2D-EIRENE simulations presented in this work, the source of neutrals crossing the separatrix was very much dominated by main chamber recycling. Neutrals recycled in the divertor were contributing much less to the pedestal fuelling even in the runs with low particle transport coefficients. We used a projection algorithm in EDGE2D-EIRENE that results in all of the ion flux arriving at the edge of the plasma grid being recycled at the wall. A different projection algorithm that redirects some fraction of the ion flux to recycle at the divertor target (for e.g. exponential fall off with an exponentially decreasing fraction going to the target) would be expected to affect the contribution from the divertor recyling to pedestal fuelling. Also, we expect that with cross-field drifts turned on, the inner divertor in the simulations would be colder and more opaque contributing significantly more to the fuelling of the pedestal [72]. In our simulations, the total amount of pedestal fuelling is experimentally constrained, but the balance between divertor and main chamber recycling is not studied in detail, which is a worthwhile line of future enquiry.

Recently, exceptional progress has been made in pedestal gyrokinetic studies [12, 73, 74, 75, 76, 77, 78, 79]. These analyses have identified various micro-instabilities to be potentially responsible for plasma transport in the H-mode pedestal. However, the focus was mostly on the understanding of the pedestal heat transport. Our work has shown that in general, inter-ELM turbulent particle transport plays an important role in setting the density pedestal. Thus, the study of micro-instabilities responsible for particle transport at the edge is a worthwhile line of future work towards a fully predictive pedestal model. Interpretative edge-SOL modelling, such as those presented in this paper, or more direct information about the particle source in the form of neutral density measurements where possible [80, 81, 82, 83] could provide information for gyrokinetic simulations to include a realistic particle source term and such advance the understanding of the density pedestal formation.

Acknowledgments

The first author would like to thank A. Chankin for fruitful discussions. This work has been carried out within the framework of the EUROfusion Consortium, funded by the European Union via the Euratom Research and Training Programme (Grant Agreement No 101052200 - EUROfusion) and from the EPSRC [grant number EP/W006839/1]. To

obtain further information on the data and models underlying this paper please contact PublicationsManager@ukaea.uk. Views and opinions expressed are however those of the authors only and do not necessarily reflect those of the European Union or the European Commission. Neither the European Union nor the European Commission can be held responsible for them.

References

[1] F. Wagner, G. Becker, K. Behringer, D. Campbell, A. Eberhagen, W. Engelhardt, G. Fussmann, O. Gehre, J. Gernhardt, G. v. Gierke, G. Haas, M. Huang, F. Karger, M. Keilhacker, O. Klüber, M. Kornherr, K. Lackner, G. Lisitano, G. G. Lister, H. M. Mayer, D. Meisel, E. R. Müller, H. Murmann, H. Niedermeyer, W. Poschenrieder, H. Rapp, H. Röhr, F. Schneider, G. Siller, E. Speth, A. Stäbler, K. H. Steuer, G. Venus, O. Vollmer, and Z. Yü. Regime of improved confinement and high beta in neutral-beam-heated divertor discharges of the ASDEX tokamak. *Phys. Rev. Lett.*, 49(19):1408–1412, 1982.

[2] M. Greenwald, R. L. Boivin, F. Bombarda, P. T. Bonoli, C. L. Fiore, D Garnier, J.A Goetz, S.N Golovato, M.A Graf, R.S Granetz, S Horne, A Hubbard, I.H Hutchinson, J.H Irby, B LaBombard, B Lipschultz, E.S Marmar, M.J May, G.M McCracken, P O Shea, J.E Rice, J Schachter, J.A Snipes, P.C Stek, Y Takase, J.L Terry, Y Wang, R Watterson, B Welch, and S.M Wolfe. H mode confinement in Alcator C-Mod. *Nuclear Fusion*, 37(6):793–807, 1997.

[3] L. D. Horton, J. P. Christiansen, J. Lingertat, C. F. Maggi, V. Mertens, O. Pogutse, G. Saibene, R. Sartori, J. Stober, W. Suttrop, The JET Team, and the ASDEX Upgrade Team. Performance near operational boundaries. *Plasma Physics and Controlled Fusion*, 41(12B):B329–B341, 1999.

[4] C. F. Maggi, R. J. Groebner, N. Oyama, R. Sartori, L. D. Horton, A.C.C. Sips, W. Suttrop, the ASDEX Upgrade Team, A. Leonard, T.C. Luce, M.R. Wade, the DIII-D Team, Y. Kamada, H. Urano, the JT-60U Team, Y. Andrew, C. Giroud, E. Joffrin, E. de la Luna, EFDA-JET Contributors for the Pedestal, Edge Physics, and the Steady State Operation Topical Groups of the ITPA. Characteristics of the H-mode pedestal in improved confinement scenarios in ASDEX Upgrade, DIII-D, JET and JT-60U. *Nuclear Fusion*, 47(7):535, 2007.

[5] P. Mantica, C. Angioni, B. Baiocchi, M. Baruzzo, M. N. A. Beurskens, J. P. S. Bizarro, R. V. Budny, P. Buratti, A. Casati, C. Challis, J. Citrin, G. Colyer, F. Crisanti, A. C. A. Figueiredo, L. Frassinetti, C. Giroud, N. Hawkes, J. Hobirk, E. Joffrin, T. Johnson, E. Lerche, P. Migliano, V. Naulin, A. G. Peeters, G. Rewoldt, F. Ryter, A. Salmi, R. Sartori, C. Sozzi, G. Staebler, D. Strintzi, T. Tala, M. Tsalas, D. Van Eester, T. Versloot, P. C. deVries, and J. Weiland. Ion heat transport studies in JET. *Plasma Physics and Controlled Fusion*, 53(12):124033, 2011.

[6] H. Zohm. Edge localized modes (ELMs). *Plasma Physics and Controlled Fusion*, 38(2):105, 1996.

[7] H. Zohm. *Magnetohydrodynamic Stability of Tokamaks*. Wiley, 2014.

[8] P. B. Snyder, H. R. Wilson, J. R. Ferron, L. L. Lao, A. W. Leonard, T. H. Osborne, A. D. Turnbull, D. Mossessian, M. Murakami, and X. Q. Xu. Edge localized modes and the pedestal: A model based on coupled peeling-ballooning modes. *Physics of Plasmas*, 9(5):2037–2043, 2002.

[9] H. R. Wilson, P. B. Snyder, G. T. A. Huysmans, and R. L. Miller. Numerical studies of edge localized instabilities in tokamaks. *Physics of Plasmas*, 9(4):1277–1286, 2002.

[10] D. Dickinson, C. M. Roach, S. Saarelma, R. Scannell, A. Kirk, and H. R. Wilson. Kinetic instabilities that limit beta in the edge of a tokamak plasma: A picture of an H-mode pedestal. *Phys. Rev. Lett.*, 108:135002, 2012.

[11] S. Saarelma, M. N. A. Beurskens, D. Dickinson, L. Frassinetti, M. J. Leyland, C.M. Roach, and EFDA-JET Contributors. MHD and gyro-kinetic stability of JET pedestals. *Nuclear Fusion*, 53(12):123012, 2013.

[12] M. Kotschenreuther, X. Liu, D. R. Hatch, S. Mahajan, L. Zheng, A. Diallo, R. Groebner, J.C. Hillesheim, C.F. Maggi, C. Giroud, F. Koechl, V. Parail, S. Saarelma, E. Solano, A. Chankin,

and and. Gyrokinetic analysis and simulation of pedestals to identify the culprits for energy losses using 'fingerprints'. *Nuclear Fusion*, 59(9):096001, 2019.

[13] E. Viezzer, E. Fable, M. Cavedon, C. Angioni, R. Dux, F.M. Laggner, M. Bernert, A. Burckhart, R.M. McDermott, T. PÃijtterich, F. Ryter, M. Willensdorfer, E. Wolfrum, and and. Investigation of inter-ELM ion heat transport in the h-mode pedestal of ASDEX upgrade plasmas. *Nuclear Fusion*, 57(2):022020, 2017.

[14] E. Viezzer, M. Cavedon, E. Fable, F.M. Laggner, R.M. McDermott, J. Galdon-Quiroga, M.G. Dunne, A. Kappatou, C. Angioni, P. Cano-Megias, D.J. Cruz-Zabala, R. Dux, T. PÃijtterich, F. Ryter, E. Wolfrum, and and. Ion heat transport dynamics during edge localized mode cycles at ASDEX upgrade. *Nuclear Fusion*, 58(2):026031, 2018.

[15] S. Mordijck. Overview of density pedestal structure: role of fueling versus transport. *Nuclear Fusion*, 60(8):082006, 2020.

[16] P. B. Snyder, R. J. Groebner, A. W. Leonard, T. H. Osborne, and H. R. Wilson. Development and validation of a predictive model for the pedestal height. *Physics of Plasmas*, 16(5):056118, 2009.

[17] P. B. Snyder, R. J. Groebner, J. W. Hughes, T. H. Osborne, M. Beurskens, A.W. Leonard, H.R. Wilson, and X.Q. Xu. A first-principles predictive model of the pedestal height and width: development, testing and ITER optimization with the EPED model. *Nuclear Fusion*, 51(10):103016, 2011.

[18] S. Saarelma, C. D. Challis, L. Garzotti, L. Frassinetti, C. F. Maggi, M. Romanelli, C. Stokes, and JET Contributors. Integrated modelling of H-mode pedestal and confinement in JET-ILW. *Plasma Physics and Controlled Fusion*, 60(1):014042, 2017.

[19] S. Saarelma, L. Frassinetti, P. Bilkova, C. D. Challis, A. Chankin, R. FridstrÃűm, L. Garzotti, L. Horvath, and C. F. Maggi. Self-consistent pedestal prediction for JET-ILW in preparation of the DT campaign. *Physics of Plasmas*, 26(7):072501, 2019.

[20] T. Luda, C. Angioni, M.G. Dunne, E. Fable, A. Kallenbach, N. Bonanomi, P.A. Schneider, M. Siccinio, G. Tardini, and and. Integrated modeling of ASDEX upgrade plasmas combining core, pedestal and scrape-off layer physics. *Nuclear Fusion*, 60(3):036023, feb 2020.

[21] A. Burckhart, E. Wolfrum, R. Fischer, K. Lackner, H. Zohm, and the ASDEX Upgrade Team. Inter-ELM behaviour of the electron density and temperature pedestal in ASDEX Upgrade. *Plasma Physics and Controlled Fusion*, 52(10):105010, 2010.

[22] F. M. Laggner, E. Wolfrum, M. Cavedon, M. G. Dunne, G. Birkenmeier, R. Fischer, M. Willensdorfer, F. Aumayr, The EUROfusion MST1 Team, and The ASDEX Upgrade Team. Plasma shaping and its impact on the pedestal of ASDEX Upgrade: edge stability and inter-ELM dynamics at varied triangularity. *Nuclear Fusion*, 58(4):046008, 2018.

[23] D. Reiter. Progress in two-dimensional plasma edge modelling. *Journal of Nuclear Materials*, 196–198:80–89, 1992.

[24] R. Simonini, G. Corrigan, G. Radford, J. Spence, and A. Taroni. Models and numerics in the multi-fluid 2-D edge plasma code EDGE2D/U. *Contributions to Plasma Physics*, 34(2–3):368–373, 1994.

[25] S. Wiesen. EDGE2D/EIRENE code interface report. *IRC Report*, 2006.

[26] G Saibene, L.D Horton, R Sartori, B Balet, S Clement, G.D Conway, J.G Cordey, H.P.L. De Esch, L.C Ingesson, J Lingertat, R.D Monk, V.V Parail, R.J Smith, A Taroni, K Thomsen, and M.G. von Hellermann. The influence of isotope mass, edge magnetic shear and input power on high density ELMy h modes in JET. *Nuclear Fusion*, 39(9):1133–1156, sep 1999.

[27] G Saibene, R Sartori, A Loarte, D J Campbell, P J Lomas, V Parail, K D Zastrow, Y Andrew, S Sharapov, A Korotkov, M Becoulet, G T A Huysmans, H R Koslowski, R Budny, G D Conway, J Stober, W Suttrop, A Kallenbach, M von Hellermann, and M Beurskens. Improved performance of ELMy h-modes at high density by plasma shaping in JET. *Plasma Physics and Controlled Fusion*, 44(9):1769–1799, aug 2002.

[28] C. D. Challis, J. Garcia, M. Beurskens, P. Buratti, E. Delabie, P. Drewelow, L. Frassinetti, C. Giroud, N. Hawkes, J. Hobirk, E. Joffrin, D. Keeling, D.B. King, C.F. Maggi, J. Mailloux, C. Marchetto, D. McDonald, I. Nunes, G. Pucella, S. Saarelma, J. Simpson, and JET Contributors. Improved confinement in JET high beta plasmas with an ITER-like wall. *Nuclear Fusion*, 55(5):053031, 2015.

[29] C. F. Maggi, S. Saarelma, F. J. Casson, C. Challis, E. de la Luna, L. Frassinetti, C. Giroud, E. Joffrin, J. Simpson, M. Beurskens, I. Chapman, J. Hobirk, M. Leyland, P. Lomas, C. Lowry, I. Nunes, F. Rimini, A.C.C. Sips, H. Urano, and JET Contributors. Pedestal confinement and stability in JET-ILW ELMy H-modes. *Nuclear Fusion*, 55(11):113031, 2015.

[30] W Suttrop, O Gruber, B Kurzan, H D Murmann, J Neuhauser, J Schweinzer, J Stober, W Treutterer, and the ASDEX Upgrade Team. Effect of plasma shape variation on ELMs and h-mode pedestal properties in ASDEX upgrade. *Plasma Physics and Controlled Fusion*, 42(5A):A97–A102, may 2000.

[31] M G Dunne, L Frassinetti, M N A Beurskens, M Cavedon, S Fietz, R Fischer, L Giannone, G T A Huijsmans, B Kurzan, F Laggner, P J McCarthy, R M McDermott, G Tardini, E Viezzer, M Willensdorfer, E Wolfrum, and and. Global performance enhancements via pedestal optimisation on ASDEX upgrade. *Plasma Physics and Controlled Fusion*, 59(2):025010, dec 2016.

[32] P.A. Schneider, C. Angioni, L. Frassinetti, L. Horvath, M. Maslov, F. Auriemma, M. Cavedon, C.D. Challis, E. Delabie, M.G. Dunne, J.M. Fontdecaba, J. Hobirk, A. Kappatou, D.L. Keeling, B. Kurzan, M. Lennholm, B. Lomanowski, C.F. Maggi, R.M. McDermott, T. PÃijtterich, A. Thorman, M. Willensdorfer, the ASDEX Upgrade Team, the EUROfusion MST1 Team, and JET Contributors. The dependence of confinement on the isotope mass in the core and the edge of AUG and JET-ILW h-mode plasmas. *Nuclear Fusion*, 62(2):026014, dec 2021.

[33] T H Osborne, J R Ferron, R J Groebner, L L Lao, A W Leonard, M A Mahdavi, R Maingi, R L Miller, A D Turnbull, M Wade, and J Watkins. The effect of plasma shape on h-mode pedestal characteristics on DIII-d. *Plasma Physics and Controlled Fusion*, 42(5A):A175–A184, may 2000.

[34] A. W. Leonard, R. J. Groebner, T. H. Osborne, and P. B. Snyder. Influence of global beta, shape, and rotation on the H-mode pedestal structure in DIII-D. *Physics of Plasmas*, 15(5):056114, 2008.

[35] H Urano, Y Kamada, H Shirai, T Takizuka, H Kubo, T Hatae, and T Fukuda. Thermal energy confinement of high-triangularity ELMy h-mode plasmas in JT-60u. *Plasma Physics and Controlled Fusion*, 44(1):11–21, nov 2001.

[36] P B Snyder and H R Wilson. Ideal magnetohydrodynamic constraints on the pedestal temperature in tokamaks. *Plasma Physics and Controlled Fusion*, 45(9):1671–1687, aug 2003.

[37] P B Snyder, H R Wilson, T H Osborne, and A W Leonard. Characterization of peeling–ballooning stability limits on the pedestal. *Plasma Physics and Controlled Fusion*, 46(5A):A131–A141, apr 2004.

[38] P.B Snyder, H.R Wilson, J.R Ferron, L.L Lao, A.W Leonard, D Mossessian, M Murakami, T.H Osborne, A.D Turnbull, and X.Q Xu. ELMs and constraints on the h-mode pedestal: peeling–ballooning stability calculation and comparison with experiment. *Nuclear Fusion*, 44(2):320–328, jan 2004.

[39] E. de la Luna, I. T. Chapman, F. Rimini, P. J. Lomas, G. Saibene, F. Koechl, R. Sartori, S. Saarelma, R. Albanese, J. Flanagan, F. Maviglia, V. Parail, A.C.C. Sips, and E.R. Solano and. Understanding the physics of ELM pacing via vertical kicks in JET in view of ITER. *Nuclear Fusion*, 56(2):026001, 2015.

[40] I T Chapman, E de la Luna, P T Lang, Y Liang, B Alper, P Denner, D Frigione, L Garzotti, C J Ham, G T A Huijsmans, S Jachmich, G Kocsis, M Lennholm, I Lupelli, F G Rimini, and A C C Sips and. Advances in understanding and utilising ELM control in JET. *Plasma Physics and Controlled Fusion*, 58(1):014017, jan 2016.

[41] A W Degeling, Y R Martin, J B Lister, L Villard, V N Dokouka, V E Lukash, and R R Khayrutdinov. Magnetic triggering of ELMs in TCV. *Plasma Physics and Controlled Fusion*, 45(9):1637–1655, aug 2003.

[42] P T Lang, A W Degeling, J B Lister, Y R Martin, P J Mc Carthy, A C C Sips, W Suttrop, G D Conway, L Fattorini, O Gruber, L D Horton, A Herrmann, M E Manso, M Maraschek, V Mertens, A MÃijck, W Schneider, C Sihler, W Treutterer, H Zohm, and ASDEX Upgrade Team. Frequency control of type-i ELMs by magnetic triggering in ASDEX upgrade. *Plasma Physics and Controlled Fusion*, 46(11):L31–L39, sep 2004.

[43] R. Pasqualotto, P. Nielsen, C. Gowers, M. Beurskens, M. Kempenaars, T. Carlstrom, D. Johnson, and JET-EFDA Contributors. High resolution Thomson scattering for Joint European Torus (JET). *Review of Scientific Instruments*, 75(10):3891–3893, 2004.

[44] Y. Andrew, N. C. Hawkes, K. Crombe, and JET EFDA Contributors. Improved charge exchange spectroscopy on the Joint European Torus for ion temperature and rotation velocity profiles. *Review of Scientific Instruments*, 77(10):10E913, 2006.

[45] E. Delabie, N. Hawkes, T. M. Biewer, and M. G. OâĂŹMullane. In situ wavelength calibration of the edge CXS spectrometers on JET. *Review of Scientific Instruments*, 87(11):11E525, 2016.

[46] R. Scannell, M. Beurskens, P. G. Carolan, A. Kirk, M. Walsh, T. O'Gorman, and T. H. Osborne. Deconvolution of Thomson scattering temperature profiles. *Review of Scientific Instruments*, 82(5):053501, 2011.

[47] G. T. A. Huysmans, J. P. Goedbloed, and W. Kerner. Isoparametric bicubic Hermite elements for solution of the Grad-Shafranov equation. In *Proceedings of the CP90 Conference on Computational Physics*, volume 02, pages 371–376, 1991.

[48] R. L. Miller, M. S. Chu, J. M. Greene, Y. R. Lin-Liu, and R. E. Waltz. Noncircular, finite aspect ratio, local equilibrium model. *Physics of Plasmas*, 5(4):973–978, 1998.

[49] A. Redl, C. Angioni, E. Belli, and O. Sauter. A new set of analytical formulae for the computation of the bootstrap current and the neoclassical conductivity in tokamaks. *Physics of Plasmas*, 28(2):022502, 2021.

[50] D. I. Réfy, M. Brix, R. Gomes, B. Tál, S. Zoletnik, D. Dunai, G. Kocsis, S. Kálvin, and T. Szabolics. Sub-millisecond electron density profile measurement at the jet tokamak with the fast lithium beam emission spectroscopy system. *Review of Scientific Instruments*, 89(4):043509, 2018.

[51] H. Weisen, A. Zabolotsky, M. Maslov, M. Beurskens, C. Giroud, D. Mazon, and JET-EFDA contributors. Scaling of density peaking in JET H-modes and implications for ITER. *Plasma Physics and Controlled Fusion*, 48(5A):A457–A466, 2006.

[52] C. Angioni, E. Fable, M. Greenwald, M. Maslov, A.G. Peeters, H. Takenaga, and H. Weisen. Particle transport in tokamak plasmas, theory and experiment. *Plasma Physics and Controlled Fusion*, 51(12):124017, 2009.

[53] A. Loarte, M. J. Leyland, J. A. Mier, M. N. A. Beurskens, I. Nunes, V. Parail, P. J. Lomas, G. R. Saibene, R. I. A. Sartori, and L. Frassinetti and. Plasma density and temperature evolution following the H-mode transition at JET and implications for ITER. *Nuclear Fusion*, 53(8):083031, 2013.

[54] G. Szepesi, L.C. Appel, E. de la Luna, L. Frassinetti, P. Gaudio, M. Gelfusa, S. Gerasimov, N.C. Hawkes, M. Sertoli, D. Terranova, and JET contributors. Advanced equilibrium reconstruction for JET with EFIT++. In *47th EPS Conference on Plasma Physics*, page P3.1037, 2021.

[55] C.D. Challis, J.G. Cordey, H. Hamnén, P.M. Stubberfield, J.P. Christiansen, E. Lazzaro, D.G. Muir, D. Stork, and E. Thompson. Non-inductively driven currents in JET. *Nuclear Fusion*, 29(4):563–570, apr 1989.

[56] L. Horvath, C.F. Maggi, A. Chankin, S. Saarelma, A.R. Field, S. Aleiferis, E. Belonohy, A. Boboc, G. Corrigan, E.G. Delabie, J. Flanagan, L. Frassinetti, C. Giroud, D. Harting, D. Keeling, D. King, M. Maslov, G.F. Matthews, S. Menmuir, S.A. Silburn, J. Simpson, A.C.C. Sips, H. Weisen, K.J. Gibson, and JET Contributors. Isotope dependence of the type i ELMy h-mode pedestal in JET-ILW hydrogen and deuterium plasmas. *Nuclear Fusion*, 61(4):046015,

2021.

[57] G. F. Matthews, P. Edwards, T. Hirai, M. Kear, A. Lioure, P Lomas, A Loving, C Lungu, H Maier, P Mertens, D Neilson, R Neu, J Pamela, V Philipps, G Piazza, V Riccardo, M Rubel, C Ruset, E Villedieu, M Way, and the ITER-like Wall Project Team. Overview of the ITER-like wall project. *Physica Scripta*, T128:137–143, 2007.

[58] J. Karhunen, M. Carr, J. R. Harrison, B. Lomanowski, I. Balboa, P. Carvalho, M. Groth, A. Huber, G. F. Matthews, A. Meakins, and S. Silburn. Effect of reflections on 2d tomographic reconstructions of filtered cameras and on interpreting spectroscopic measurements in the jet iter-like wall divertor. *Review of Scientific Instruments*, 90(10):103504, 2019.

[59] Dr Carine Giroud, Dr Alex Meakins, Dr Matthew Carr, Dr Alfonso Baciero, and Mr Corentin Bertrand. CHERAB Spectroscopy Modelling Framework, https://doi.org/10.5281/zenodo.1206142, 2018.

[60] Carr M et al. Towards integrated data analysis of divertor diagnostics with ray-tracing. In *44th EPS Conference on Plasma Physics*, page O5.130, 2017.

[61] Dr Alex Meakins and Matthew Carr. raysect/source: Release 0.5.5, https://doi.org/10.5281/zenodo.2583254, 2019.

[62] H P Summers, W J Dickson, M G O Mullane, N R Badnell, A D Whiteford, D H Brooks, J Lang, S D Loch, and D C Griffin. Ionization state, excited populations and emission of impurities in dynamic finite density plasmas: I. the generalized collisional–radiative model for light elements. *Plasma Physics and Controlled Fusion*, 48(2):263–293, jan 2006.

[63] E de la Cal, U Losada, A Martín de Aguilera, A Shaw, E Solano, D Alegre, I Balboa, P Carvalho, J Gaspar, I Borodkina, S Brezinsek, D Douai, C Giroud, C Guillemaut, C Hidalgo, A Huber, E Joffrin, T Loarer, E de la Luna, A Manzanares, F Militello, L de Pablos, and S Wiesen and. Impact of divertor configuration on recycling neutral fluxes for ITER-like wall in JET h-mode plasmas. *Plasma Physics and Controlled Fusion*, 62(3):035006, jan 2020.

[64] E. A. Belli and J. Candy. Kinetic calculation of neoclassical transport including self-consistent electron and impurity dynamics. *Plasma Physics and Controlled Fusion*, 50(9):095010, 2008.

[65] E. A. Belli and J. Candy. Full linearized Fokker-Planck collisions in neoclassical transport simulations. *Plasma Physics and Controlled Fusion*, 54(1):015015, 2012.

[66] E. A. Belli, G. W. Hammett, and W. Dorland. Effects of plasma shaping on nonlinear gyrokinetic turbulence. *Physics of Plasmas*, 15(9):092303, 2008.

[67] A Marinoni, S Brunner, Y Camenen, S Coda, J P Graves, X Lapillonne, A Pochelon, O Sauter, and L Villard. The effect of plasma triangularity on turbulent transport: modeling TCV experiments by linear and non-linear gyrokinetic simulations. *Plasma Physics and Controlled Fusion*, 51(5):055016, mar 2009.

[68] O. Beeke, M. Barnes, M. Romanelli, M. Nakata, and M. Yoshida. Impact of shaping on microstability in high-performance tokamak plasmas. *Nuclear Fusion*, 61(6):066020, may 2021.

[69] J. W. Hughes, B. LaBombard, D. A. Mossessian, A. E. Hubbard, J. Terry, T. Biewer, and the Alcator C-Mod Team. Advances in measurement and modeling of the high-confinement-mode pedestal on the alcator c-mod tokamak. *Physics of Plasmas*, 13(5):056103, 2006.

[70] J.W Hughes, B LaBombard, J Terry, A Hubbard, and B Lipschultz. Edge profile stiffness and insensitivity of the density pedestal to neutral fuelling in alcator c-mod edge transport barriers. *Nuclear Fusion*, 47(8):1057–1063, aug 2007.

[71] R. Reksoatmodjo, S. Mordijck, J.W. Hughes, J.D. Lore, and X. Bonnin. The role of edge fueling in determining the pedestal density in high neutral opacity alcator c-mod experiments. *Nuclear Materials and Energy*, 27:100971, 2021.

[72] M Groth, G D Porter, T D Rognlien, S Wiesen, M Wischmeier, M N A Beurskens, X Bonnin, B D Bray, S Brezinsek, N H Brooks, D P Coster, T Eich, M E Fenstermacher, C Fuchs, R A Groebner, D Harting, A Huber, S Jachmich, A Kallenbach, C J Lasnier, A W Leonard, A Meigs, H W MÃijller, M E Rensink, D L Rudakov, J G Watkins, E Wolfrum, and and. Poloidal distribution of recycling sources and core plasma fueling in DIII-d, ASDEX-upgrade and JET l-mode plasmas.

Plasma Physics and Controlled Fusion, 53(12):124017, nov 2011.

[73] D. R. Hatch, M. Kotschenreuther, S. Mahajan, P. Valanju, F. Jenko, D. Told, T. GÃűrler, and S. Saarelma. Microtearing turbulence limiting the JET-ILW pedestal. *Nuclear Fusion*, 56(10):104003, 2016.

[74] D. R. Hatch, M. Kotschenreuther, S. Mahajan, P. Valanju, and X. Liu. A gyrokinetic perspective on the JET-ILW pedestal. *Nuclear Fusion*, 57(3):036020, 2017.

[75] M. Kotschenreuther, D.R. Hatch, S. Mahajan, P. Valanju, L. Zheng, and X. Liu. Pedestal transport in H-mode plasmas for fusion gain. *Nuclear Fusion*, 57(6):064001, 2017.

[76] D. R. Hatch, M. Kotschenreuther, S. M. Mahajan, G. Merlo, A.R. Field, C. Giroud, J.C. Hillesheim, C.F. Maggi, C. Perez von Thun, C.M. Roach, S. Saarelma, and JET Contributors. Direct gyrokinetic comparison of pedestal transport in JET with carbon and ITER-like walls. *Nuclear Fusion*, 59(8):086056, 2019.

[77] Jason F. Parisi, Felix I. Parra, Colin M. Roach, Carine Giroud, William Dorland, David R. Hatch, Michael Barnes, Jon C. Hillesheim, Nobuyuki Aiba, Justin Ball, Plamen G. Ivanov, and JET contributors. Toroidal and slab ETG instability dominance in the linear spectrum of JET-ILW pedestals. *Nuclear Fusion*, 60(12):126045, oct 2020.

[78] D.R. Hatch, M. Kotschenreuther, S.M. Mahajan, M.J. Pueschel, C. Michoski, G. Merlo, E. Hassan, A.R. Field, L. Frassinetti, C. Giroud, J.C. Hillesheim, C.F. Maggi, C. Perez von Thun, C.M. Roach, S. Saarelma, D. Jarema, F. Jenko, and JET Contributors. Microtearing modes as the source of magnetic fluctuations in the JET pedestal. *Nuclear Fusion*, 61(3):036015, feb 2021.

[79] B. Chapman, D.R. Hatch, A.R. Field, J.C. Hillesheim, L. Horvath, C.F. Maggi, C.M. Roach, S. Saarelma, L. Frassinetti, J. Walker, and JET contributors. The role of slab-etg modes in jet-ilw pedestals with varying levels of power and fuelling. *in preparation*, 2021.

[80] A. M. Rosenthal, J. W. Hughes, A. Bortolon, F. M. Laggner, T. M. Wilks, R. Vieira, R. Leccacorvi, E. Marmar, A. Nagy, C. Freeman, and D. Mauzey. A 1d lyman-alpha profile camera for plasma edge neutral studies on the diii-d tokamak. *Review of Scientific Instruments*, 92(3):033523, 2021.

[81] F. M. Laggner, A. Bortolon, A. M. Rosenthal, T. M. Wilks, J. W. Hughes, C. Freeman, T. Golfinopoulos, A. Nagy, D. Mauzey, and M. W. Shafer. Absolute calibration of the lyman-Îś measurement apparatus at diii-d. *Review of Scientific Instruments*, 92(3):033522, 2021.

[82] A. M. Rosenthal et al. Calculation of pedestal transport using direct measurements of neutral emissivity on DIII-D. In *25th Joint EU-US Transport Task Force Meeting*, 2021.

[83] F. Sciortino, N.T. Howard, R. Reksoatmodjo, A.R. Foster, J.W. Hughes, E.S. Marmar, M.A. Miller, S. Mordijck, T. Odstrcil, T. Putterich, M.L. Reinke, J.E. Rice, and P. Rodriguez-Fernandez. Experimental inference of neutral and impurity transport in alcator c-mod using high-resolution x-ray and ultra-violet spectra. *submitted to Nuclear Fusion*, 2021.